Observation of Multifractality in Anderson Localization of Ultrasound

Sanli Faez,[1,*] Anatoliy Strybulevych,[2] John H. Page,[2] Ad Lagendijk,[1] and Bart A. van Tiggelen[3]

[1]*FOM Institute for Atomic and Molecular Physics AMOLF, Science Park 113, 1098 SJ Amsterdam, The Netherlands*
[2]*Department of Physics and Astronomy, University of Manitoba, Winnipeg, Manitoba, R3T 2N2, Canada*
[3]*Université Joseph Fourier, Laboratoire de Physique et Modélisation des Milieux Condensés, CNRS,
25 Rue des Martyrs, BP 166, 38042 Grenoble, France*

We report the experimental observation of strong multifractality in wave functions below the Anderson localization transition in open three-dimensional elastic networks. Our results confirm the recently predicted symmetry of the multifractal exponents. We have discovered that the result of multifractal analysis of real data depends on the excitation scheme used in the experiment.

PACS numbers: 64.60.al, 05.70.Jk, 42.25.Dd, 43.35.+d

Critical phenomena are of prominent importance in condensed-matter physics. Criticality at the Anderson localization transition has been the subject of intensive theoretical research. Some important theoretical predictions have been made, among which is the remarkable aspect of multifractality of wave functions at this transition. Numerical simulations support these predictions but also raise more questions [1]. Recent experimental progress has paved the way for the direct investigation of the Anderson localization transition at the mobility edge in real samples [2–4].

In this Letter, we report the experimental observation of strong multifractality (MF) just below the Anderson transition. This observation is based on the excitation of elastic waves in an open 3D disordered medium. The recently predicted symmetry relation of the MF exponents [5] is tested and confirmed. All results are compared with the corresponding analysis of diffusive (metallic) wave functions in the same network at a different frequency or with a light speckle pattern generated by a strongly scattering medium, showing a very clear difference between localizing and diffusive regimes. Our results not only highlight the presence of MF in wave functions close to the mobility edge, but also reveal new aspects of the MF character in real experimental systems.

Before presenting the experimental results, we briefly review some general aspects of MF and their implications in the context of the Anderson transition. Multifractality quantifies the strong fluctuations of the wave function. It shows the nontrivial length-scale dependence of the moments of the intensity distribution. The dependence can be investigated by varying the system size L, or alternatively, if the system size is fixed, by dividing the system into small boxes of linear size b and varying b. This property is quantified by using the generalized inverse participation ratios (GIPR)

$$P_q = \sum_{i=1}^{n} (I_{B_i})^q = \sum_{i=1}^{n} \left[\int_{B_i} I(\mathbf{r}) d^d \mathbf{r} \right]^q, \qquad (1)$$

where $I(\mathbf{r})$ is the normalized intensity (equal to $|\psi^2(\mathbf{r})|/\int |\psi^2(\mathbf{r})| d^d r$ where $\psi(\mathbf{r})$ is the wave function) and I_{B_i} is the integrated probability inside a box B_i of linear size b, with $\lambda \ll b \ll L$ where λ is the wavelength. The summation is performed on the whole sample, which consists of $n = (L/b)^d$ boxes, and d is the space dimension. By definition $P_1 \equiv 1$ and $P_0 \equiv n$.

At criticality, the ensemble averaged GIPR, $\langle P_q \rangle$, scales anomalously with the dimensionless scaling length L/b as

$$\langle P_q \rangle \sim (L/b)^{-d(q-1)-\Delta_q} \equiv (L/b)^{-\tau(q)}, \qquad (2)$$

where $d(q-1)$ and Δ_q are called the normal (Euclidean) and the anomalous dimensions, respectively. For a normal (extended) wave function, $\Delta_q = 0$ for every q. A (single-) fractal wave function with fractal dimension D is described by $\tau(q) \equiv D(q-1)$. For critical states $\tau(q)$ is a continuous function of q that fully describes the MF.

MF describes the scaling of the moments of a probability density function (PDF). The GIPR, defined in Eq. (1), are proportional to the moments of the distribution function of the eigenfunction intensities, so that Eq. (2) implies the following scaling relation for the PDF:

$$\mathcal{P}(\ln I_B) \sim (L/b)^{-d+f(-[\ln I_B/\ln(L/b)])}. \qquad (3)$$

The second term in the exponent, $f(\alpha)$, is called the singularity spectrum, and is related to the set of anomalous exponents $\tau(q)$ by a Legendre transform

$$\tau(q) = q\alpha - f(\alpha), \qquad q = f'(\alpha), \qquad \alpha = \tau'(q). \quad (4)$$

The singularity spectrum $f(\alpha)$ is the fractal dimension of the set of those points $\mathbf{r}$ where the wave-function intensity, $I(\mathbf{r})$, scales as $L^{-\alpha}$. In mathematical terms, it shows the coexistence of several populations of singularities in the measure, which is the wave-function intensity for this specific case. In the field-theoretical treatment of random-Schrödinger Hamiltonians, MF implies the presence of infinitely many relevant operators [6,7]. The functional dependence of $f(\alpha)$ is an important and unique property

of each universality class. In the extended regime, $\mathcal{P}(\ln I_B)$ is strongly peaked near $\alpha = d$, since the short-range "Gaussian" fluctuations [8] are washed out in the box integration.

First order perturbation theory for an Anderson transition in $2 + \epsilon$ dimensions [9] (two is the critical dimension), results in the "parabolic approximation" for the MF wave functions [10,11]. This result, $\Delta_q = \gamma q(1 - q)$, corresponds to $f(\alpha) = d - (\alpha - d - \gamma)^2/4\gamma$, where γ is a constant in the order of ϵ. A similar approximation applies to metallic (diffusive) states in three dimensions [12,13] due to weak localization, although with $\gamma \ll 1$. This is sometimes called weak MF.

Recently, an exact symmetry relation

$$\Delta_q = \Delta_{1-q}, \qquad (5)$$

was theoretically predicted for the set of anomalous exponents [5]. The numerical and analytical investigations of the 3D Anderson model and certain random matrices suggest that MF may exhibit itself also for off-critical states on both sides of the transition [14]. The MF concept was extended to the boundaries where it behaves differently with respect to the bulk [15].

Most of the available information about MF is based on numerical investigations (See, e.g., [1,16–18] and references therein). The only experimental attempt to observe strong MF in wave functions so far is due to Morgenstern *et al.* using scanning tunneling microscopy of 2D electron systems [2]. Their observation of MF was hindered by the presence of several eigenfunctions in the measurement and by the limited size of their system.

We now use ultrasonic measurements to demonstrate three different, but closely related, manifestations of MF: (i) the probability density function (PDF), (ii) the scaling of generalized inverse participation ratios (GIPR), and (iii) direct extraction of the singularity spectrum. Our experiments were performed on disordered single-component elastic networks, made by brazing randomly-packed 4.11-mm-diameter aluminium beads together [3]. The data presented here were obtained from a representative disc-shaped sample with a 120 mm diameter and 14.5 mm thickness. Two different configurations were used for excitation. In the first excitation scheme a point-like ultrasound source emits short pulses next to the sample surface. In the second case the source was put far from the sample so that a quasiplanar wave was incident on the whole interface. In close proximity to the opposite interface, vibrational excitations of the network were probed with sub-wavelength-diameter detectors in the frequency range of 0.2 to 3 MHz, where the wavelengths are comparable to the bead size and the scattering mean free paths are much less than the sample thickness [3]. The intensity at a particular frequency was determined from the square of the magnitude of the Fourier transform of the entire time-dependent transmitted field in each near-field speckle.

The intensity was normalized by the total intensity in the measured speckle pattern. The normalized speckle intensity, $I(j)$ was recorded at each point j on a square grid of linear size $L_g = 55$ points with a typical nearest-neighbor spacing of 0.66 mm.

In the lower frequency band around 250 kHz, the ultrasound propagation is diffusive. A localizing regime is observed in a 50% bandwidth around 2.4 MHz, where the measured localization length in the sample is smaller than the size of the analyzed speckle patterns ($0.7L_g$) and almost equal to the sample thickness. A full description of the experiment and a thorough comparison of previous measurements with the self-consistent theory of localization has been presented in [3].

We obtain the PDF from the histogram of the logarithm of box-integrated intensities I_{B_i}. We sample over 100 speckles in a 5% bandwidth around 250 kHz and 2.4 MHz for diffusive and localized regimes, respectively. Two representative histograms are shown in Fig. 1 with typical box sizes of $b = 9$ and $b = 2$ points for low and high frequency measurements, corresponding to box sizes of approximately two wavelengths in both cases. The PDF for localized waves is clearly much wider than the one for diffusive waves and the peak is shifted from the average intensity. We have also plotted the peak-position and the width of the histogram as a function of box size in the inset of Fig. 1.

In principle, it is possible to extract the MF spectrum from the PDF [19]. However, a box-counting analysis can give more accurate results based on the scaling of the GIPR. Similar to many numerical studies, we approximate the expectation values by box sampling over a single or multiple wave functions measured for a single realization of disorder. This approximation is known as typical aver-
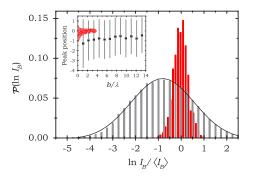

FIG. 1 (color online). Comparison between coarse-grained PDF for localized and diffusive speckle intensities. The PDFs are experimentally obtained from the histogram of the logarithm of averaged intensities in the localized (thick bars) and diffusive (thin bars) regimes. The black line shows a fit to a single parameter log-normal distribution given by the parabolic approximation of Eq. (3). Inset: The peak position (symbols) and the full width at half maximum (bars) of the intensity histogram is plotted for localized (circles) and diffusive (squares) speckles as a function of coarse-graining box size.

aging. Typical averaging is unable to reveal information that is related to statistically rare events [1]. In this approach, the system size is fixed and supposed to be large enough relative to the box size. The approximate scaling relation is derived by plotting the estimated GIPR, given by Eq. (1), versus the box size b [20]. Note that although we have examined three-dimensional samples, the Euclidian dimension of our sampling space is two since the available data are taken just from the surface of the sample. The effective system size is L_g over which the intensities are normalized. By plotting P_q versus the box size in bilogarithmic scales [e.g., see the inset to Fig. 2(a)], power-law behavior is found for $q \in [-3, 4]$, with the slope yielding the scaling exponent $\tau(q)$. The average anomalous exponent is obtained by averaging the exponents measured for several frequencies between 2.0 and 2.6 MHz and subtracting off the normal part of the exponent $2(q-1)$. The standard deviation is taken as the error bar.

The anomalous exponents are plotted as a function of q in Fig. 2(a). For comparison with the localized data, the same numerical procedure was applied to a diffusive speckle pattern, where the behavior is entirely different ($\Delta_q = 0$). In making this comparison, an optical diffusive speckle pattern was used to capitalize on the best available statistics.

The behavior of the anomalous exponents shown in Fig. 2 provides unambiguous evidence for surface MF of the localized ultrasound wave functions. This is the most important result in this Letter. Note that MF is clearly seen in these data, even though the localized wave functions in our finite sample are near to, but not exactly at, criticality. In addition, our observation of MF clearly supports the predicted symmetry relation (5). Our experimental dem-
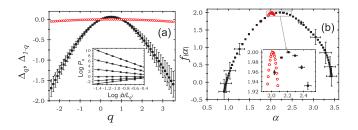
onstration of this fundamental symmetry, seen in a very different system to the ones envisaged in [5], attests to the universality of critical properties near the Anderson transition.

Finally, we have extracted the surface MF spectrum directly from the measurements [21]. In this method the numerical error caused by the Legendre transform (4) is avoided. To get enough statistics, 100 wave functions in a bandwidth of 5% are used to estimate the MF spectrum for several seven frequency bands between 2.0 and 2.6 MHz. No systematic deviation is observed between the seven spectra obtained in this frequency range. These spectra are then averaged for each value of $q \in [-6, 6]$ and the standard deviation is considered as the error bar. The results are summarized in Fig. 2(b). The peak of the MF spectrum is shifted from two (the Euclidian dimension of the measurement basis) by a value of 0.21 ± 0.02. For comparison, the same procedure is applied to the optical speckle using the same q range. No shift is observed for the optical speckle.

The MF that is clearly seen in our data allows us to test the deviation from the parabolic approximation. This is characterized by the reduced anomalous exponents $\delta_q \equiv \frac{\Delta_q}{q(1-q)}$. In our results, shown in Fig. 3(a), we see a deviation of less than 20% for $q \in [-3, 4]$. The nonparabolicity of the spectrum is very difficult to measure but it may have important theoretical consequences. More precise investigation of larger samples is needed to reliably confirm or exclude the possibility of a small but significant deviation.

We have also investigated the dependence of the reduced anomalous exponent at the symmetry axis, $\delta_{1/2} = 4\Delta_{1/2}$, on the frequency and type of excitation. The results are presented in Fig. 3(b). We observe a robust presence of MF for all frequencies between 1.7 to 2.9 MHz. The measured anomalous exponent is larger for the point source illumination. This difference may be related to the number of modes excited in each scheme. It has been previously
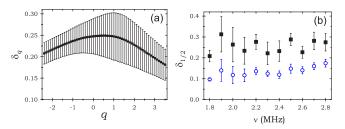

FIG. 2 (color online). (a) The measured anomalous exponents Δ_q are shown for localized ultrasound (full squares) and diffusive light (open circles) speckles. The dashed line shows the same data-points, mirrored relative to $q = \frac{1}{2}$ in order to check the symmetry in the spectrum. The anomalous exponents are estimated from the box-counting method. The slope of the GIPR plotted versus the box size in bilogarithmic scales yields Δ_q. One example is shown in the inset for $q \in \{-2, -1, 0, 1, 2, 3\}$ and $f = 2.40$ MHz. (b) The average singularity spectrum is calculated for the ultrasound speckles (full squares) at frequencies between 2.0 to 2.6 MHz. For comparison a singularity spectrum for diffusive optical speckle (open circles), with the Euclidian dimension, is extracted by applying the same box-counting procedure.

FIG. 3 (color online). (a) The reduced anomalous dimension $\delta_q \equiv \frac{\Delta_q}{q(1-q)}$ is plotted versus q. Bars show the estimated error. Deviation from a horizontal line corresponds to the deviation from parabolic approximation. (b) The reduced anomalous dimension $\delta_{1/2}$ is plotted versus frequency in the localized regime for two excitation schemes: point-source (squares) and plane wave (circles). The error bars represent the standard deviation of the measured exponents that are averaged over each 0.1-MHz-wide frequency band.

discussed [22] that the overlap of two or more eigenmodes shifts the peak of the singularity spectrum towards the Euclidian dimension. Since the surface area of the sample is larger than the localization length, neighboring localized modes may coexist at the same frequency. These modes can all be excited by a quasiplane wave while a point source couples more efficiently to the closest mode.

Numerical analyses of bulk and surface MF for the eigenstates of the Anderson tight-binding Hamiltonian on a 3D cubic lattice at the metal-insulator transition have predicted corresponding shifts of 1.0 and 1.6 from the Euclidean dimension for the peak of the singularity spectrum [19,23]. Another numerical study for an equivalent vibrational model on the *fcc* lattice shows a similar outcome for bulk MF [18], indicating to the universality of this phenomenon. It is not simple to explain the difference between the available numerical results and our experimental outcome. Several issues may play a role. Mode overlap and the finite lifetime of modes due to open boundaries are two of these issues. Most numerical studies are done based on uncorrelated disorder, which is experimentally hardly ever achieved. The uniform bead size in our samples, which is comparable with the vibrational wavelength, is a source of correlation. The presence of correlation in the disordered potential may influence the critical behavior and induce nonuniversality [24].

Despite the wealth of theoretical and numerical studies on the Anderson transition in 2D and 3D for the Schrödinger Hamiltonian in closed systems, critical properties of this transition for classical waves in an open system have never been studied. Our system is specially challenging due to its 3D nature, open boundaries and presence of three polarizations for the elastic waves. Specific properties of classical waves such as absorption are yet to be investigated in the context of criticality. Our results show that these important questions can now be investigated experimentally, providing vital guidance for new theoretical work. Our experiments reveal that the concept of MF not only concerns critical states but is valid as well around the mobility edge. This observation agrees with recent theoretical investigations [14]. Mutual avoidance of wave functions at large energy separations and their enhanced overlap at small energy separations are other important predictions of that theory, which can also be verified by our experiment.

In conclusion, we have presented the first experimental observation of multifractal wave functions below the localization transition. Our data validate experimentally the predicted symmetry relation of the anomalous exponents. Free from interactions and with the possibility of diverse illumination and detection schemes, sound and light experiments can provide a tremendous amount of useful information for this field of research. We believe that our observation of multifractality in classical waves will stimulate new theoretical and numerical investigations. On the experimental side, this work highlights again the strength of statistical methods for studying Anderson localization.

*faez@amolf.nl

[1] F. Evers and A. D. Mirlin, Rev. Mod. Phys. **80**, 1355 (2008).

[2] M. Morgenstern, J. Klijn, C. Meyer, and R. Wiesendanger, Phys. Rev. Lett. **90**, 056804 (2003).

[3] H. Hu, A. Strybulevych, J. H. Page, S. E. Skipetrov, and B. A. van Tiggelen, Nature Phys. **4**, 945 (2008).

[4] J. Chabe, G. Lemarie, B. Gremaud, D. Delande, P. Szriftgiser, and J. C. Garreau, Phys. Rev. Lett. **101**, 255702 (2008).

[5] A. D. Mirlin, Y. V. Fyodorov, A. Mildenberger, and F. Evers, Phys. Rev. Lett. **97**, 046803 (2006).

[6] B. Duplantier and A. W. W. Ludwig, Phys. Rev. Lett. **66**, 247 (1991).

[7] C. Mudry, C. Chamon, and X.-G. Wen, Nucl. Phys. **B466**, 383 (1996).

[8] B. Shapiro, Phys. Rev. Lett. **57**, 2168 (1986).

[9] F. Wegner, Z. Phys. B **36**, 209 (1980).

[10] H. Aoki, J. Phys. C **16**, L205 (1983).

[11] C. Castellani and L. Peliti, J. Phys. A **19**, L429 (1986).

[12] B. L. Al'tshuler, V. E. Kravtsov, and I. V. Lerner, Sov. Phys. JETP **64**, 1352 (1986).

[13] V. I. Falko and K. B. Efetov, Phys. Rev. B **52**, 17 413 (1995).

[14] E. Cuevas and V. E. Kravtsov, Phys. Rev. B **76**, 235119 (2007).

[15] A. R. Subramaniam, I. A. Gruzberg, A. W. W. Ludwig, F. Evers, A. Mildenberger, and A. D. Mirlin, Phys. Rev. Lett. **96**, 126802 (2006).

[16] H. Grussbach and M. Schreiber, Phys. Rev. B **51**, 663 (1995).

[17] A. Mildenberger and F. Evers, Phys. Rev. B **75**, 041303 (2007).

[18] J. J. Ludlam, S. N. Taraskin, and S. R. Elliott, Phys. Rev. B **67**, 132203 (2003).

[19] A. Rodriguez, L. J. Vasquez, and R. A. Römer, Phys. Rev. Lett. **102**, 106406 (2009).

[20] We have used box sizes $b \in \{2, 3, 4, 6, 8, 12, 24\}$.

[21] A. Chhabra and R. V. Jensen, Phys. Rev. Lett. **62**, 1327 (1989).

[22] T. Terao, T. Nakayama, and H. Aoki, Phys. Rev. B **54**, 10 350 (1996).

[23] C. Monthus and T. Garel, Phys. Rev. B **80**, 024203 (2009).

[24] I. F. dos Santos, F. A. B. F. de Moura, M. L. Lyra, and M. D. Coutinho-Filho, J. Phys. Condens. Matter **19**, 476213 (2007).